ce/papers Proceedings in civil engineering

Ernst & Sohn A Wiley Brand

Full paper

General Formulation for the Buckling Resistance of Uniform and Non-Uniform Slender I-Section Beams

José Osvaldo Ferreira Filho[1] | Luís Simões da Silva[1] | Trayana Tankova[2] | Hermes Caravalho[2]

Correspondence

Dr. José Osvaldo Ferreira Filho
University of Coimbra
Department of Civil Engineering
Rua Luís Reis Santos – Pólo II
3030-788, Coimbra, Portugal
Email: jose.filho@dec.uc.pt

[1] University of Coimbra, ISISE, ARISE, Department of Civil Engineering, Coimbra, Portugal
[2] Delft University of Technology, Department of Engineering Structures, Delft, Netherlands
[3] University of São Paulo, Department of Civil Engineering, São Paulo, Brazil

Abstract

The General Formulation has proven to be a practical, design-focused solution for the stability design of different member configurations - built-up or not, uniform or non-uniform, with complex or simple support conditions. It was recently extended for mono-symmetric I-section beams, but its applicability to slender section members remains unexplored. This work aims to expand the scope of the General Formulation to include Class 4 I-section beams. A numerical model was calibrated to assess the lateral-torsional buckling resistance of beams. A parametric study was conducted on S690 HSS slender I-section beams under uniform bending moment, considering different cross-sections, normalized slenderness, prismatic and non-prismatic beams, simply-supported and arbitrary boundary conditions. Finally, the numerical results were compared to the analytical ones of the General Formulation and Eurocode 3, supporting the applicability of the General Formulation due to its good correlation with the numerical model.

Keywords

Stability, Complex Members, Slender Sections, Eurocode 3, High-Strength Steel

1 Introduction

The second generation of Eurocode 3 (EC3) [1], introduces the new method for Lateral-Torsional Buckling (LTB) proposed by Taras and Greiner [2], which serves as an alternative of the General Case for doubly-symmetric I-section beams under fork boundary conditions at both ends. The approach leads to well estimated results and was recently extended for mono-symmetric I-section beams [3], but it is not applied for members under arbitrary boundary conditions or with variable cross-sections along the length. For such members, the use of the General Method is recommended by the code, but has been appointed in the literature [4,5] as inconsistent and very time-consuming since it depends on non-linear analyses.

In response to these limitations, Tankova et al. [6] proposed a General Formulation (GF) that allow for the verification of generic single members, built-up or not, uniform or not, with complex support conditions or not. This approach has proven to be a practical, design-focused solution, relying solely on linear buckling analyses (LBA), and it was recently extended for mono-symmetric I-section beams [7]. However, it has only been validated for compact and semi-compact sections, and its application for slender sections remains unexplored.

This paper aims to extend the General Formulation to deal with uniform and non-uniform slender I-section beams with arbitrary boundary conditions submitted to uniform bending moment. The buckling resistance of members with varying sections and slenderness is investigated using a calibrated numerical model. The numerical results are then compared with analytical results derived from the General Case (GC) and General Method (GM) in EC3 [1], as well as from the extended General Formulation, to assess the accuracy of each approach.

2 Extension of the General Formulation for Slender Sections

The General Formulation (GF) adopts the Ayrton-Perry design philosophy in a raw format of a linear interaction equation, in which the first- and second-order normal stresses are included and the global reduction factor, χ, is not applied. There is no need to calibrate additional parameters, such as the critical location and loading factors. The critical buckling mode obtained from a previous LBA is used as the shape of the initial

https://doi.org/10.1002/cepa.70087

imperfection and the pertinent eigenvalues - critical load multiplier, α_{cr}, critical transverse displacements along z-axis, w_{cr}, and y-axis, v_{cr}, and critical twist rotation, θ_{cr}, etc. - are used to calculate the second-order contributions. The developed interaction equation should be applied for all potential failure modes and the verification should be performed for a sufficient number of cross-sections along the member, including the end sections.

The utilization ratio of a generic single member can be calculated by dividing the total longitudinal stress, σ, from the first- and second-order forces - axial force, $N(x)$, first and second-order out-of-plane bending moments, $M_z(x)$ and $M_z^{II}(x)$, first and second-order in-plane bending moments, $M_y(x)$ and $M_y^{II}(x)$, and bi-moment, $M_w^{II}(x)$ - to the yield stress, f_y. The verification of a single member with arbitrary geometry, boundary conditions and loading is performed checking if Eq. (1) is satisfied.

$$\frac{N(x)}{A_i(x)f_y}+\frac{M_y(x)}{W_{y,i}(x)f_y}+\frac{M_z(x)}{W_{z,i}(x)f_y}+\frac{M_y^{II}(x)}{W_{y,i}(x)f_y}+\frac{M_z^{II}(x)}{W_{z,i}(x)f_y}+\frac{M_w^{II}(x)}{W_w(x)f_y}\leq 1.0 \quad (1)$$

where $A_i(x)$ is the relevant cross-section area, $W_{y,i}(x)$ and $W_{z,i}(x)$ are the relevant section moduli relative to the y- and z-axes, respectively, which are defined according to Table 1 extracted from clause 8.2.2.6 of EC3 [1], and $W_w(x)$ is the warping modulus at location x along the member obtained according Eq. (2).

Table 1 Section properties according to the class of the cross-section

Class	Area A_i	Moment of inertia I_y	Moment of inertia I_z	Section modulus W_y	Section modulus W_z
1	A	I_y	I_z	$W_{pl,y}$	$W_{pl,z}$
2	A	I_y	I_z	$W_{pl,y}$	$W_{pl,z}$
3	A	I_y	I_z	$W_{el,y}{}^*$	$W_{el,z}{}^*$
4	A_{eff}	$I_{y,eff}$	$I_{z,eff}$	$W_{eff,y}{}^*$	$W_{eff,z}{}^*$

* The elastic section modulus corresponds to the extreme fibre with the maximum elastic stress.

$$W_w(x)=\frac{C_w(x)}{w_{max}(x)} \quad (2)$$

where $C_w(x)$ is the warping constant and $w_{max}(x)$ is the maximum sectorial area.

Differently from Tankova et al. [6] and Gomes Jr et al. [7], where only compact and semi-compact cross-sections were contemplated, in this work, as Class 4 cross-sections are analysed, the effective properties of the sections (Figure 1) should be calculated to consider the effects of the local buckling.

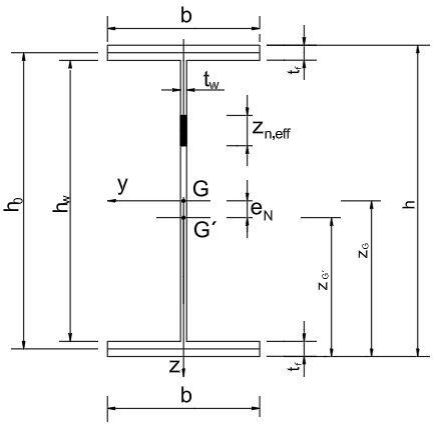

Figure 1 Typical effective doubly-symmetric I-section beam

In contrast to Eurocode 3, the general formulation dismisses the need of previously identifying the buckling mode, since the potential critical displacements - w_{cr}, v_{cr}, and θ_{cr} - cannot simultaneously occur. Consequently, the verification process aligns with a particular buckling case.

Concerning LTB, the components of the critical buckling mode shape are $v_{cr}(x)$ and $\theta_{cr}(x)$, and the general interactions exhibited in Eq. (1) becomes:

$$\frac{\sigma(x)}{f_y}=\frac{M_y(x)}{W_{y,i}(x)f_y}+\frac{M_z^{II}(x)}{W_{z,i}(x)f_y}+\frac{M_w^{II}(x)}{W_w(x)f_y} \quad (3)$$

The second-order contributions from $M_z^{II}(x)$, which depends on the lateral displacement, $v(x)$, and $M_w^{II}(x)$, which depends on the twist rotation, $\theta(x)$, are calculated by Eqs. (4) and (5).

$$M_z^{II}(x)=-EI_{z,i}(x)v"(x) \quad (4)$$

$$M_w^{II}(x)=-EC_w(x)\theta"(x) \quad (5)$$

In the case of tapered beams, an additional warping component from the inclination of the flanges is added leading the Eq. (5) to:

$$M_w^{II}(x)=-EC_w(x)\left[\theta"(x)+\frac{2}{\mathrm{h}}\theta'(x)h'\right] \quad (6)$$

In a complex configuration concerning members with different geometries, and boundary and loading conditions, the imperfection cannot be determined as in the new LTB method [2], i.e. by coupling the lateral displacement and the twist rotation, as it is done for simply supported beams [8]. Consequently, it was decided to adopt the both critical components of the mode shape, $v_{cr}(x)$ and $\theta_{cr}(x)$, as initial imperfections, scaling them by the same amplitude. Then, the initial lateral displacement, $v_0(x)$, and the initial twist rotation, $\theta_0(x)$, are calculated using Eq. (7) and (8), respectively:

$$v_0(x)=v_{cr}(x)\bar{\delta}_{0,LTB} \quad (7)$$

$$\theta_0(x)=\theta_{cr}(x)\bar{\delta}_{0,LTB} \quad (8)$$

The resulting amplification relationship for lateral displacement, $v(x)$, and twist rotation, $\theta(x)$, is expressed by:

$$v(x) = \frac{1}{\alpha_{cr}-1} v_0(x) \quad (9)$$

$$\theta(x) = \frac{1}{\alpha_{cr}-1} \theta_0(x) \quad (10)$$

From the assumption that the real beam has the same buckling resistance of an equivalent simply supported beam, with the same geometry at the critical cross-section, x_m, and the same elastic critical bending moment, M_{cr}, the second-order utilization factors for both can be equalled and the required amplitude of the generalized imperfection can be determined. It is further assumed that the location x_m is the location where $v"_{cr}$ reaches the maximum values along the beam.

The second-order utilization factor for the equivalent beam at the critical cross-section, x_m, is given by:

$$\varepsilon_M^{II}(x_m) = \frac{M_z^{II}(x_m)}{W_{z,i}(x_m) f_y} + \frac{M_w^{II}(x_m)}{W_w(x_m) f_y} = \frac{\alpha_{cr} M_{y,Ed}(x_m) \bar{e}_0 \theta_{cr}(x_m)}{W_{z,i}(x_m) f_y (\alpha_{cr}-1)} \left(1 + \frac{v_{cr}(x_m)}{\theta_{cr}(x_m)} \frac{W_{z,i}(x_m)}{W_w(x_m)} + \frac{GJ(x_m)}{M_{cr}} \frac{W_{z,i}(x_m)}{W_w(x_m)}\right) = \frac{N_{cr,z} \bar{e}_0}{W_{z,i}(x_m) f_y (\alpha_{cr}-1)} \quad (11)$$

From Eqs. (4) and (5), the second-order utilization factor for the real beam at the same location is expressed by:

$$\varepsilon_M^{II}(x_m) = \frac{M_z^{II}(x_m)}{W_{z,i}(x_m) f_y} + \frac{M_w^{II}(x_m)}{W_w(x_m) f_y} = \frac{EI_{z,i}(x_m) \bar{\delta}_0}{W_{z,i}(x_m) f_y (\alpha_{cr}-1)} \left[v''_{cr}(x_m) + \frac{W_{z,i}(x_m)}{W_w(x_m)} \frac{C_w(x_m)}{I_{z,i}(x_m)} \left(\theta"_{cr}(x_m) + \frac{2}{h} \theta'_{cr}(x_m) h'\right)\right] \bar{\delta}_0 \quad (12)$$

For Class 4 cross-sections with slender flanges, the Eq. (12) becomes:

$$\varepsilon_M^{II}(x_m) = \frac{M_z^{II}(x_m)}{W_{z,i}(x_m) f_y} + \frac{M_w^{II}(x_m)}{W_w(x_m) f_y} = \frac{EI_{z,i}(x_m)(v"_{cr}(x_m) + h\theta"_{cr}(x_m) + 2\theta'_{cr}(x_m) h') \bar{\delta}_0}{W_{z,i}(x_m) f_y (\alpha_{cr}-1)} \quad (13)$$

As:

$$\frac{W_{z,i}(x_m)}{W_w(x_m)} \frac{C_w(x_m)}{I_{z,i}(x_m)} = \frac{\frac{I_{z,i}(x_m)}{\rho_f b^2} C_w(x_m)}{\frac{C_w(x_m)}{w_{max}(x)} I_{z,i}(x_m)} = \frac{\frac{2}{\rho_f b}}{\frac{4}{hb}} = \frac{h}{2\rho_f} \quad (14)$$

The difference between Eqs. (12) and (13) is the application of the reduction factor for the flange plate buckling, ρ_f, which is equal 0.5 or 1.0, when the flange is slender or not, respectively.

For slender cross-sections, equalling Eqs. (11) and (13) yields the amplitude of the imperfection related to lateral-torsional buckling, $\bar{\delta}_{0,LTB}$, Eq. (15), that contains the equivalent geometrical imperfection, $\bar{e}_0$, and additional terms establishing the consistency with EC3 [1] stability design rules.

$$\bar{\delta}_{0,LTB} = \frac{N_{cr,z} \bar{e}_0}{EI_{z,i}(x_m)\left[v"_{cr}(x_m) + \frac{h}{2\rho_f}\left(\theta"_{cr}(x_m) + \frac{2}{h}\theta'_{cr}(x_m) h'\right)\right]} = f_\eta \bar{e}_0 \quad (15)$$

Following [6], $\bar{e}_0$ is given by Eq. (16):

$$\bar{e}_0 = \alpha_{LT}(x_m)\left(\bar{\lambda}(x_m) - 0.2\right) f_\eta |\delta_{cr}(x_m)| \frac{W_{z,i}(x_m)}{A_i(x_m)} \quad (16)$$

where $\alpha_{LT}(x_m)$ is the imperfection factor related to the LTB from EC3 [1], $\bar{\lambda}(x_m)$ is the non-dimensional slenderness at a given position, the factor f_η is given by Eq. (17) and $\delta_{cr}(x_m)$ is the general displacement of the critical mode found by a geometric relationship between the lateral displacement and the rotation of the section (Figure 2), which is expressed by Eq. (18).

$$f_\eta = \frac{N_{cr,z}}{EI_{z,i}(x_m)\left[v"_{cr}(x_m) + \frac{h}{2\rho_f}\left(\theta"_{cr}(x_m) + \frac{2}{h}\theta'_{cr}(x_m) h'\right)\right]} \quad (17)$$

$$\delta_{cr}(x) = v_{cr}(x) + \left(\frac{h(x)}{2} + e_N\right)\theta_{cr}(x) \quad (18)$$

Finally, the utilization ratio $\varepsilon_M(x)$ can be expressed and the generalized imperfection factor, $\eta(x)$, is expressed by Eqs. (19) and (20):

$$\varepsilon_M(x) = \frac{M_{y,Ed}(x)}{W_{y,i}(x) f_y} + \frac{EI_{z,i}(x)\left[v''_{cr}(x) + \frac{h}{2\rho_f}\left(\theta"_{cr}(x) + \frac{2}{h}\theta'_{cr}(x) h'\right)\right]}{A_i(x) f_y (\alpha_{cr}-1)} \eta(x) \leq 1.0 \quad (19)$$

$$\eta(x) = \alpha_{LT}(x)\left(\bar{\lambda}(x) - 0.2\right) f_\eta |\delta_{cr}(x)| \quad (20)$$

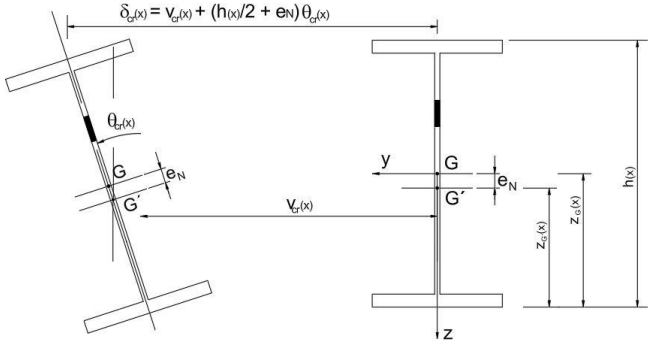

Figure 2 General displacement of the critical mode

Using the differential equation for flexural buckling - Eq. (21) -, the equivalent elastic critical force for out-of-plane buckling, $N_{cr,z,eq}$, is "retrieved" – Eq. (22):

$$EI_z(x) v''_{cr}(x) + N_{cr,z,eq} v_{cr}(x) = 0 \quad (21)$$

$$N_{cr,z,eq} = \frac{EI_{z,i}(x_m)|v''_{cr}(x_m)|}{|v_{cr}(x_m)|} \quad (22)$$

This force is the one used herein for the calculation of the normalized slenderness – Eq. (23):

$$\bar{\lambda}(x) = \sqrt{\frac{A_i(x) f_y}{N_{cr,z,eq}}} \quad (23)$$

3 Numerical study

3.1 Finite Element (FE) model

The numerical model was developed in ABAQUS [9] and it is a simple extension of the numerical model proposed by Ferreira Filho et al. [10] for beams. The geometry of the models was simulated considering the nominal dimensions and overlaps between the parts of the cross-sections at the web-flange junctions were avoided using tie

constraints, which could also allow adequate connection. Figure 3 illustrated the base geometry of the model, showing the main geometrical parameters. As observed, he longitudinal welds between the web and the flanges were not modelled without loss of accuracy, as corroborated by previous studies [11].

The true stress-strain curve of the material was represented according to EC3-1-14 [12]. The four-node finite element with full integration S4 was implemented and the mesh was composed by 16 elements across the flanges' width and other 16 across the web's depth, in agreement with previous studies [11].

The fork boundary conditions were simulated following the recommendations of Snijder et al. [13]. The restrictions to lateral and vertical displacements were inserted at the nodes coincident with the centroids of each end-section, as well as the restrictions to torsional rotation. At one side, the longitudinal displacements were also prevented at the centroid node (Figure 4a). In both ends, all nodes of each flange were coupled for all displacements and rotations to its middle node. The same was done for the web, but without coupling the nodes for the rotations around the vertical axis, which was responsible to turn the end sections infinitely rigid and able to warp (Figure 4b). The end bending moments were applied at the centroid nodes.

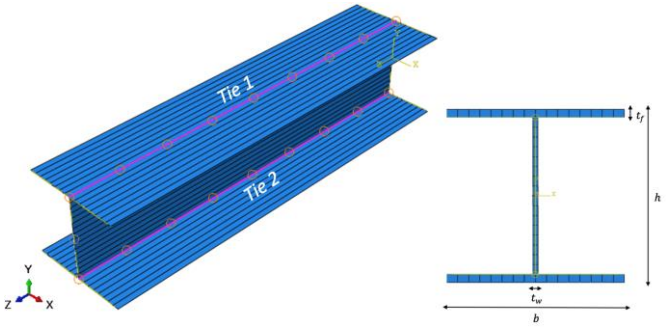

Figure 3 Reference geometry of the numerical models

(a)

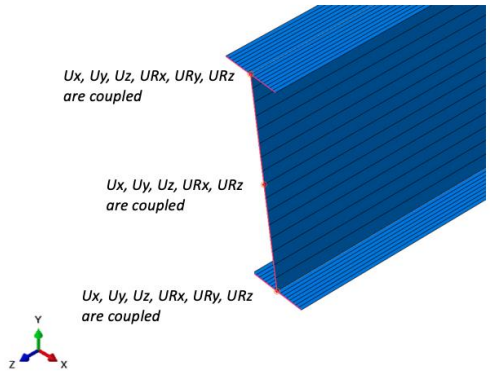

(b)

Figure 4 Boundary conditions (a) and constraints (b) applied to the numerical model to simulate the fork-supported beams

The initial geometrical imperfections were introduced with a shape related to LTB eigenmode from previous linear buckling analyses (LBA) and amplitude equal to L/1000, as recommended by ECCS [14]. The pattern and magnitude of the membrane residual stresses were adopted according to the novel model proposed by Schaper et al. [15] for welded I-section members with thermal-cut flanges.

3.2 Validation

Finally, the numerical model was compared to the experimental results on class 4 welded I-section beams executed in project STROBE [16], in which the main information of the members is given in details. The deviations from the results are shown in Table 2, in which good agreement was found between the numerical model and the experimental tests. Reasonable correlation was also achieved between the curves of vertical load *versus* vertical displacements, as observed in Figure 5. Furthermore, the same failure modes found in the experimental tests were reproduced by the numerical model. In Figure 6, the lateral-torsional buckling, which was the failure mode found for all members, is illustrated with different perspective views.

Table 2: Experimental versus numerical results for ultimate load

Prototype	Ult. Resistance (kN)		Deviation
	EXP	FEM	$\frac{FEM}{EXP}$
B5	1024.5	1018.3	0.99
B7	1384.6	1395.2	1.01
B8	1327.9	1329.2	1.00
B11	1731.8	1822.7	1.05
B12	1601.0	1620.1	1.01
B13	1307.2	1331.4	1.02
B14	1133.3	1142.8	1.01

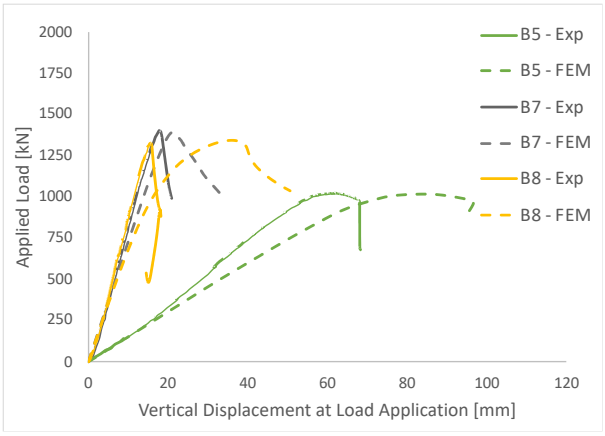

(a)

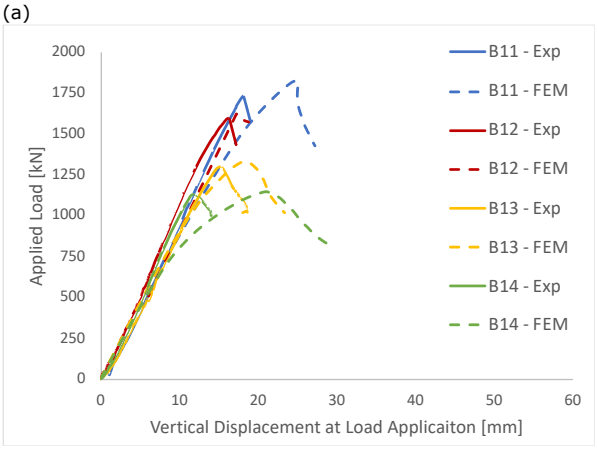

(b)

Figure 5 Comparison between load versus displacement curves for the doubly-symmetric (a) and monosymmetric (b) beams

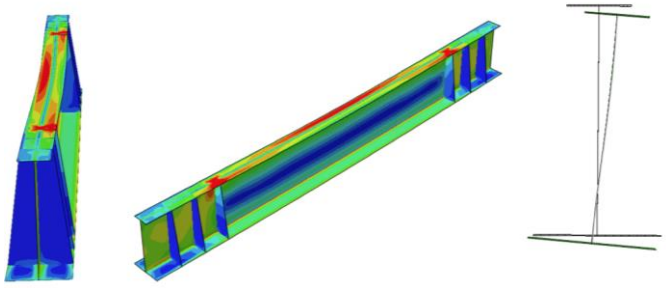

Figure 6 Typical LTB failure mode (Example of beam B11)

3.3 Parametric study

A parametric study on prismatic and non-prismatic Class 4 I-section beams under constant bending moment was executed, considering the class 4 sections for the steel grade S690 (Table 3). Stocky to slender members were analyzed with non-dimensional slenderness, $\bar{\lambda}_z$, varying from 1.0 to 7.0. Three types of boundary conditions further the fork supports were considered (Figure 7).

Table 3: Experimental versus numerical results for ultimate load

Type	Section 1 $h \times b \times t_w \times t_f$ (mm)	Section 2 $h \times b \times t_w \times t_f$ (mm)	h_1/h_2
Uniform	700x200x8x16	700x200x8x16	1.00
Uniform	850x200x8x16	850x200x8x16	1.00
Uniform	925x200x8x16	925x200x8x16	1.00
Uniform	1000x200x8x16	1000x200x8x16	1.00
Non-Uniform	850x200x8x16	700x200x8x16	1.21
Non-Uniform	925x200x8x16	700x200x8x16	1.32
Non-Uniform	1000x200x8x16	700x200x8x16	1.43
Non-Uniform	925x200x8x16	850x200x8x16	1.16
Non-Uniform	1000x200x8x16	850x200x8x16	1.25
Non-Uniform	1000x200x8x16	925x200x8x16	1.08

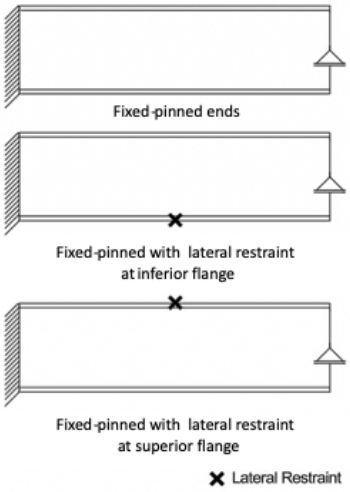

Figure 7 Arbitrary boundary conditions

4 Validation of GF for slender sections

The results from the numerical model were compared to the analytical results from the General Formulation (GF) and EC3 [1]. The scatter plot of r_t versus r_e is shown for all sections covered herein, where r_e is the ratio between the numerical and plastic resistance, and r_t is the ratio between the analytical and the plastic resistance. The results for the uniform beams under fork supports is exhibited in Figure 8, whilst the ones for uniform beams under the arbitrary boundary conditions, in Figure 9. The results for the tapered beams are illustrated in Figure 10.

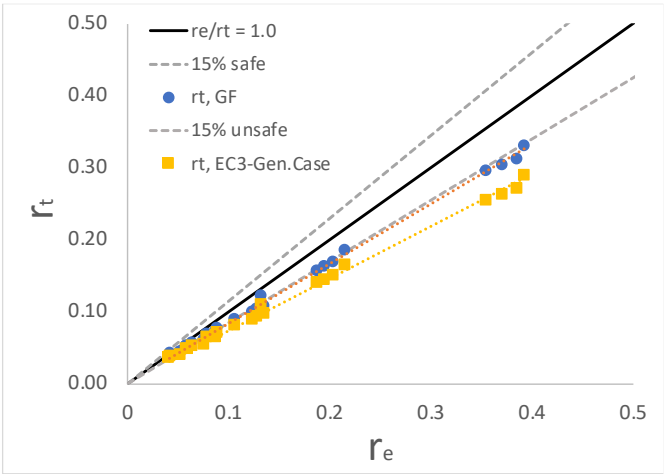

Figure 8 Numerical versus analytical results for uniform beams with fork supports

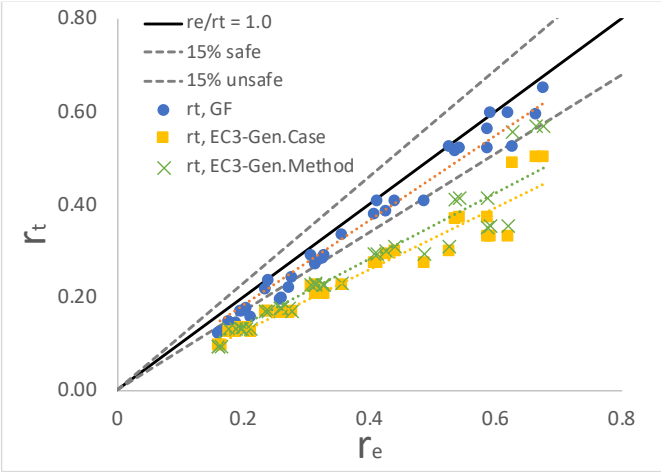

Figure 9 Numerical versus analytical results for uniform beams with arbitrary boundary conditions

As observed in Figure 7, both analytical methodologies provided safe-sided results for the simply-supported beams. Concerning the average of ratios r_N (analytical over numerical resistance), the GF correlates better with the numerical model, showing an average r_N of 1.15, while General Case displayed conservative results with an average r_N equal to 1.34.

For the results of beams under arbitrary boundary conditions (Figure 8), better agreement is found using the GF over the approaches of EC3 [1]. The GF showed an average r_N equal to 1.15, whist General Case and General Method exhibited 1.55 and 1.48, respectively.

The GF also reached better results than the General Method for the tapered members with an average r_N of 1.18, while using GM leaded to an average r_N of 1.44.

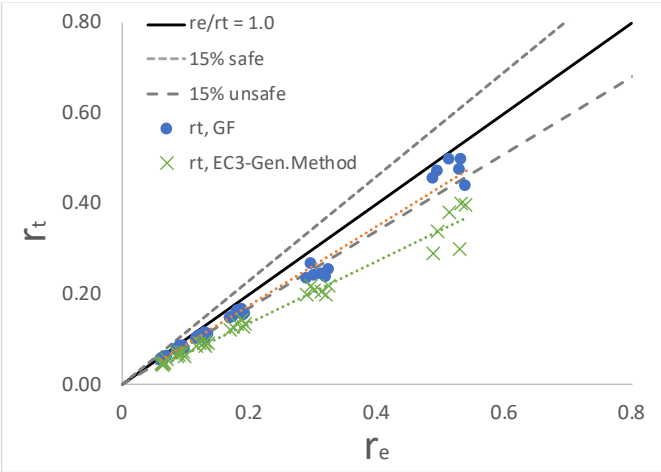

Figure 10 Numerical versus analytical results for tapered beams

5 Conclusions

In this paper, the General Formulation (GF) proposed by Tankova et al. [6] was extended to deal with slender I-section beams. The numerical model built by Ferreira Filho et al. [10] was calibrated to run a parametric study of S690 slender I-section beams, in which 192 members were analysed and the LTB numerical resistances were compared to the analytical results from GF and EC3. The comparisons showed that the GF displays safe-sided results for all the range of members and it agrees better with the numerical model than the approaches from EC3. Finally, it is concluded that the GF can be a practical solution to deal with complex configurations of geometry and boundary conditions over the General Method. However, the parametric study presented here is limited, and a more general numerical study should be executed involving also different loads, steel grades, and also very stocky members.

References

[1] EN 1993-1-1. (2022) *Eurocode 3 - Design of Steel Structures – Part 1-1*: General Rules and Rules for Buildings. Brussels: Comité Européen de Normalisation (CEN).

[2] Taras, A.; Greiner, R. (2010) *New design curves for lateral-torsional buckling – proposal based on a consistent derivation*. Journal of Constructional Steel Research 66(5):648-663.

[3] Simões da Silva, L.; Gomes Junyor, J.O.; *Ferreira Filho, J.O.;* Carvalho, H. (2025). *Ayrton-Perry approach for the lateral-torsional buckling resistance of mono-symmetric I-section beams*. Thin-Walled Structures, 211, 113125. https://doi.org/10.1016/j.tws.2025.113125.

[4] Marques, L.; Simões da Silva, L.; Greiner, R.; Rebelo, C.; Taras, A. (2013) Development of a consistent design procedure for lateral-torsional buckling of tapered beams. Journal of Constructional Steel Research, 89, pp. 213-235.

[5] Simões da Silva, L.; Marques, L.; Rebelo, C. (2010) *Numerical validation of the general method in EC3-1-1: lateral, lateral-torsional and bending and axial force interaction of uniform members*. Journal of Constructional Steel Research, 66, pp. 575-590 (2010), http://dx.doi.org/10.1016/j.jcsr.2009.11.003

[6] Tankova, T.; Simões da Silva, L.; Marques, L. (2018) *Buckling resistance of non-uniform steel members based on stress utilization: general formulation*. *Journal of Constructional Steel Research*, 149, 239-256 (2018)

[7] Gomes Jr., J. O; Simões da Silva, L.; Tankova, T.; Carvalho, H.; Ferreira Filho, J.O. (2023) *Lateral-torsional buckling resistance of non-prismatic and prismatic monosymmetric I-section steel beams based on stress utilization*. Engineering Structures, 305, 117758. https://doi.org/10.1016/j.engstruct.2024.117758.

[8] Chen, F.; Astuta, T. (1977) *Theory of Beam-Columns Vol. 2: Space behaviour and design*. McGraw-Hill.

[9] Abaqus v. 6.21. (2021), Dassault Systems/Simulia, Providence, RI, USA.

[10] Ferreira Filho, J.O.; Tankova, T.; Carvalho, H.; Martins, C.; Simões da Silva, L. (2022) *Experimental and numerical flexural buckling resistance of high strength steel columns and beam-columns*. Engineering Structures, 265, 114414.

https://doi.org/10.1016/j.engstruct.2022.114414.

[11] Ferreira Filho, J.O.; Simões da Silva, L.; Tankova, T.; Carvalho, H. (2023) *Influence of geometrical imperfections and residual stresses on the reliability of high strength steel welded I-section columns using Monte Carlo simulation*. Journal of Constructional Steel Research, 215, 108548. https://doi.org/10.1016/j.jcsr.2024.108548.

[12] prEN 1993-1-14. (2022) *Eurocode 3: Design of steel structures – Part 1-14: Design assisted by finite element analysis*, Brussels: Comité Européen de Normalisation (CEN).

[13] Snijder, H.H.; van der A, R.P.; Hofmeyer, H.; van Hove, B. W. E. M. (2018) *Lateral torsional buckling design imperfections for use in non-linear FEA*. Steel Construction, 11, 49-56.

[14] ECCS. (1984) *Ultimate Limit State Calculation of Sway Frames with Rigid Joints*, Brussels: Publication No.33.

[15] Shaper, L.; Tankova, T.; Simões da Silva, L.; Knobloch, M. (2022) *A novel residual stress model for Welded I-sections*, Journal of Constructional Steel Research, 188, 107017.

[16] Tankova, T.; Rodrigues, F.; Leitão, C.; Martins, C.; Simões da Silva, L. (2021) *Lateral-torsional buckling of high strength steel beams: Experimental resistance*, Thin-Walled Struct. 164 (2021) 107913.